

Computational Design of a Kit of Parts for Bending-Active Structures

ANONYMOUS AUTHOR(S)
SUBMISSION ID: 837

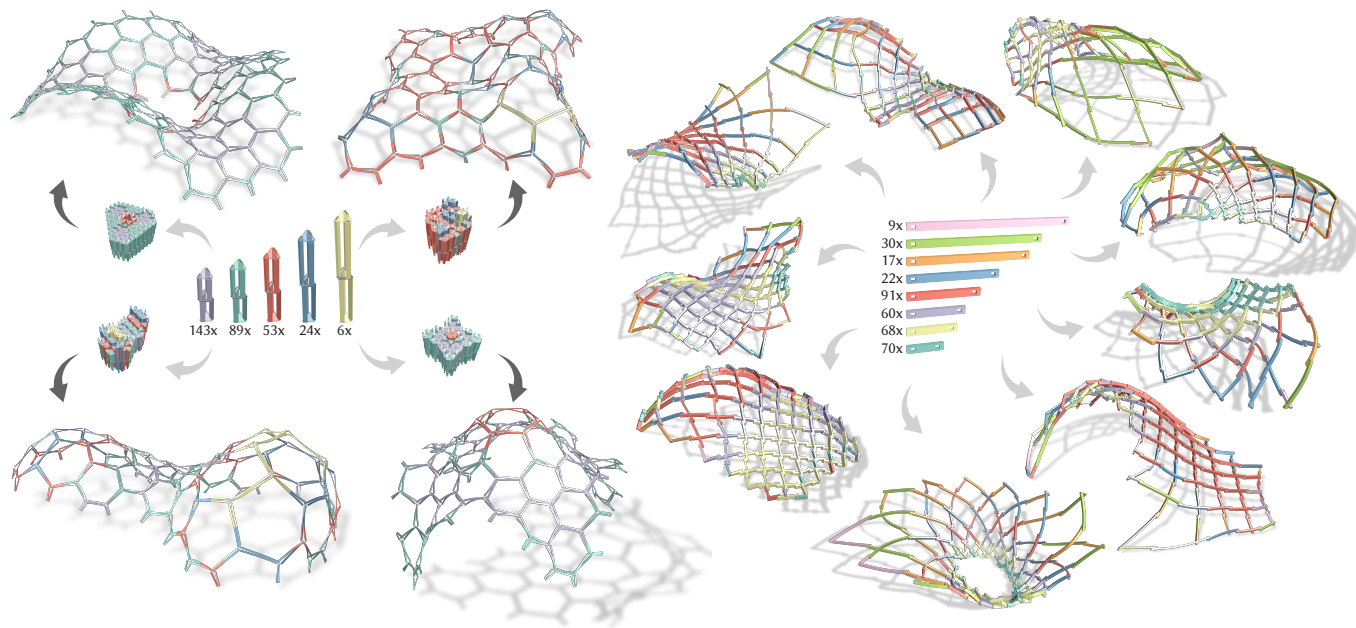


Fig. 1. A kit of parts allows cost-effective fabrication of bending-active assemblies. Our general optimization method finds the part geometries to best reproduce a given set of input designs and can be specialized to different material systems. Left: Umbrella meshes deploy from a compact assembly state towards a target equilibrium. Right: Bending-active orthogonal gridshells assembled from straight beams that deform to best approximate the target surface.

Bending-active structures are composed of elastic elements that deform to achieve a desired target shape. To support effective design, inverse algorithm have been proposed that optimize the geometry of each individual element specifically for each design. This makes it difficult to re-use elements across designs or gain efficiency in fabrication through mass production.

We address this issue and propose a computational framework to rationalize bending-active structures into a sparse kit of parts. Our method solves for the optimal part geometry such that multiple input designs can be faithfully realized with the same kit of parts. Assigning parts to different assemblies leads to a combinatorial explosion that makes exhaustive search intractable. Instead, we propose a relaxed continuous optimization that incorporates a physics-based simulation in its inner loop to accurately model the elastic deformation of the bending-active structure. Our algorithm allows analyzing different design trade-offs of a kit of parts to tune the balance between fabrication complexity and fidelity to the original designs. We demonstrate our method on three different classes of bending-active structures, showcasing the effectiveness of our approach for part reuse and sustainable practices in fabrication-driven design.

Additional Key Words and Phrases: kit of parts, bending-active structures, numerical optimization, physics-simulation, fabrication

1 INTRODUCTION

Bending-active structures are physical systems characterized by distinctive curved geometries, which arise from the elastic deformation of initially straight or planar elements. This formation approach not only enables the creation of static structures but also facilitates

the construction of kinetic and deployable systems by leveraging the reversibility of elastic deformations [Lienhard 2014]. While the constituent elements must be thin and slender to allow significant deformation, the structures must counterbalance this material reduction to withstand loads by employing alternative stress-stiffening effects achieved through appropriate geometric design [La Magna 2017].

The equilibrium form of these structures emerges when all internal forces induced by elastic deformation of the elements and external forces, such as gravity, are in global balance. The presence of large deformations, along with the sensitivity of the structural form to even minor changes in the geometry and material properties of its constituents, makes the design process highly challenging. In response to this, physics-based simulations have been integrated into the research of bending-active structures to accurately predict equilibrium states [Lienhard et al. 2013; Manolas et al. 2022]. To match a simulated form with a desired input freeform geometry, inverse design algorithms have been proposed that directly solve for the design parameters of the bending-active structure [Becker et al. 2023; Panetta et al. 2019; Pillwein and Musialski 2021; Ren et al. 2022]. These parameters typically define the undeformed rest state of the constituent elements, which can be fabricated in a flat state and then assembled into the final structure.

One key advantage of bending-active structures is that their constituent elements are designed to maintain strain within the elastic limits of the material, allowing for reversible elastic deformation. This means that a structure can be undeployed and individual components could in principle be re-used in a different design. However, current inverse design methods compute optimized component geometries that are specific to one particular design only. This limits the re-use potential of parts and requires custom fabrication of each individual element, which can be slow and expensive compared to mass production techniques. Our work addresses these drawbacks and investigates the question of how to design a kit of parts that can be manufactured at scale and be re-used across multiple designs of bending-active structures.

This problem has been extensively studied for static structures composed of rigid components, in particular in the context of architectural research [Alegria Mira et al. 2016; Brütting et al. 2021]. Freeform designs are rendered feasible for fabrication by *rationalizing* them to groups of identical components. Such an optimized kit of parts can be used to assemble complex structures with an efficient fabrication pipeline, providing a cheaper and more sustainable alternative to custom fabrication. We study this problem for bending-active structures, where parts can deform into many different configurations in different assemblies. This additional complexity requires a fundamentally different approach.

Contributions. Our main contribution is a computational framework for optimizing a kit of parts for bending-active structures. We propose a numerical method that relaxes the discrete combinatorial nature of the part-to-element assignment problem into a continuous optimization problem. This fully differentiable optimization can be seamlessly combined with a physics-based simulation that tracks the equilibrium states of all input design instances mapped onto the kit of parts. Our formulation is general in that it can be applied to different classes of bending-active structures. We show how to customize the algorithm for three concrete examples of bending-active structures, highlighting the versatility of our approach. [The full source code and experiments can be found at https://github.com/???](https://github.com/???).

2 RELATED WORK

We discuss prior work on bending-active and deployable structures in the context of component reuse and rationalization. Works proposing component reuse in architecture are followed by a review of reconfigurable systems with reusable components as their building blocks. We mention computational methods for rationalization in the context of computer graphics and further narrow our focus on modular involving a kit-of-parts approach to conclude the section.

Deployable Structures. Deployable structures transform from a compact *rest* state that is typically easy to assemble, transport, and store to a *deployed* target state. While deployment mechanisms span across different scales and material systems [Yang et al. 2023], we focus on structures composed of elastic beams coupled via specific joining mechanisms. Trusses, space frames, and gridshells [Dyvik et al. 2021] are notable examples of such structures on an architectural scale. Several works deal with finding deployable variants of gridshells [Panetta et al. 2019; Pillwein and Musalski 2021; Schling

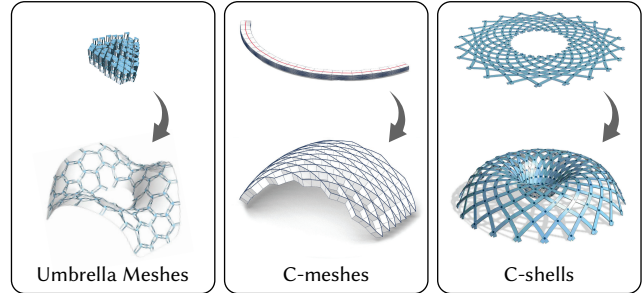


Fig. 2. Examples of structures using bending-active beams (Umbrella Meshes [Ren et al. 2022], C-shells [Becker et al. 2023]) and orthogonal grids (a superset of C-meshes [Liu et al. 2023b]) that can be deployed into a 3D target surface.

et al. 2022; Tellier 2022] and the actuation sequence for their erection. The inverse-design problem of computing the rest state that deploys to a desired deployed state is of particular interest. Approaches involving geometric abstractions and numerical optimization have been proposed to solve the problem for different deployable structures [Baek et al. 2018; Becker et al. 2023; Liu et al. 2023b; Ren et al. 2022].

Figure 2 shows a few deployable structures that have bending active deployments. While digital fabrication techniques have enabled the creation of bespoke solutions tailored to specific deployment states, our focus shifts to optimizing kit of parts that can be reused across multiple designs and deployments. This shift to generalized kits introduces significant challenges. Specifically, the inherent difficulty of rationalizing a material system is further intensified by the large deformations characteristic of bending-active structures. In these cases, the complexity is twofold: ensuring that the structure’s deployability is preserved throughout the rationalization process, and accurately maintaining and tracking the equilibrium states of the system.

Orthogonal Gridshells. Another subset of bending-active structures that is of particular interest are orthogonal gridshells where the beam profiles are oriented normal to the design surface, allowing beams to deform along their weak axis to approximate the surface geometry, while load transfer occurs locally via their strong axis [Schling 2018]. Networks of asymptotic curves to create asymptotic gridshells [Schling and Barthel 2020; Schling et al. 2022], pseudo-geodesic gridshells [Mesnil et al. 2023] are examples of such structures using straight strips. Circular strips have also been used on surfaces of constant mean curvature [Schling et al. 2018], or for deployable orthogonal structures (along with straight ones) through the concept of C-meshes [Liu et al. 2023b]. We consider a generalization of these structures with curved planar lamellae.

Re-usable Structures. Our focus on a kit-of-parts addresses the challenge of promoting the reusability of structural components. Although recycling supports material reuse, reusing components and entire structures conserves significantly more energy and resources [Allwood et al. 2012; Iacovidou and Purnell 2016]. Reuse-driven design [Fivet and Brütting 2020; Huang et al. 2021] is crucial for

229 promoting component reuse both upstream (by procuring components
 230 for future use) and downstream (by designing with future
 231 reuse in mind). An interesting approach of re-usability are mod-
 232 ular structures made of identical universal components that can
 233 be reconfigured for various design realizations. Alegría and co-
 234 workers [2016] introduce a universal scissor component that can be
 235 reconfigured to all basic scissor cells. Liu et al. [2022] use recon-
 236 figurable units with three multi-stable states (long, short, and bent) to
 237 design 3D space metawires for reconfigurable antennas. Kusupati
 238 and colleagues [2023] use identical, shape-agnostic, and recon-
 239 figurable umbrella cells to realize structures that deploy into a large
 240 range of desired geometries. Although universal reconfigurable com-
 241 ponents can be manufactured at scale and reused across various
 242 designs, they often involve significant complexity in terms of part
 243 geometry and fabrication. In contrast, our work adopts the principle
 244 that a simpler, less reconfigurable kit of parts can be mass-produced
 245 more cost-effectively, striking a balance between part reuse and
 246 fabrication complexity.

247 *Computational Rationalization.* An important aspect of our work
 248 involves the rationalization of target geometries into a finite set of
 249 parts. A lot of research is currently being carried out in computer
 250 graphics and computational geometry that is relevant for the pan-
 251 elization of free-form surfaces [Liu et al. 2021; Singh and Schaefer
 252 2010; Zhu et al. 2023] with applications in architecture [Egensatz
 253 et al. 2010; Zimmer et al. 2012]. Fu and colleagues [2010] generate a
 254 set of K quads whose instances can produce a tiled quad surface that
 255 approximates the input surface. Freeform honeycomb structures
 256 [Jiang et al. 2014] provide a torsion-free support structure with iden-
 257 tical nodes. Jiang et al. [2021] use panels that are manufacturable by
 258 precise isometric bending of surfaces made from a small number of
 259 molds of constant Gaussian curvature. Various works such as [Luo
 260 et al. 2015; Testuz et al. 2013; Zhang and Balkcom 2016] also explore
 261 volumetric rationalization of 3D shapes using shape filling blocks.

262 Other works focus on clustering the set of parts based on dif-
 263 ferent metrics. Basso and colleagues [2009] perform an optimiza-
 264 tion on free-form gridshells to cluster elements into a predefined
 265 number of different length groups. Liu et al. [2023a] present a clus-
 266 tering-optimization framework to reduce the number of different
 267 nodes in space frame structures. Zimmer and co-workers [2014] ra-
 268 tionalize free-form shapes to a single kit of parts using the *Zometool*
 269 set. A set made of linear elements of nine different lengths connected
 270 by one universal joint with different connection directions. Lu and
 271 Xie [2023] reduce the number of different members in a truss layout
 272 by considering shared lengths between members as well as shared
 273 cross-sections. Schling and Barthel [2020] provide a holistic theory
 274 of *repetitive structures* considering both the geometric and construc-
 275 tive parameters through computational design. Their systematic
 276 study aims to identify principle relationships of form and structure
 277 and develop new design strategies.

278 *Kit-of-Parts Approach.* It is not a new idea to use a kit of parts
 279 pre-designed and engineered to be mass-produced for construction.
 280 Howe et al. [1999] draw parallels to an object-oriented programming
 281 environment with well-defined interfaces to be followed (e.g. load
 282 transfer rules, cost constraints, boundary constraints). Brüttig and
 283 colleagues [2021] present a new computational workflow to design

284 a bespoke kit of parts that can be employed to build structures of
 285 diverse typologies using optimization of structural members and
 286 joints i.e., the kit of parts, that fit multiple geometric and structural
 287 requirements. St-Hilaire and Nejur [2022] propose form-matching
 288 of a temporary architectural structure with a kit of parts coupling
 289 wood with simple bendable steel strips. Gaudreault and Nejur [2023]
 290 introduce a constructive system aimed at maximizing the integration
 291 of reclaimed materials for the construction of triangular reticular
 292 structures. While these works take a kit-of-parts design approach,
 293 they do not handle free-form bending-active structures. We provide
 294 a general framework for rationalizing bending-active structures
 295 employing physics-based simulation for form-finding in the inner
 296 loop of the optimization.

3 OVERVIEW

300 Bending-active structures based on elastically deforming beams
 301 share many commonalities, even when their deployment mecha-
 302 nism are fundamentally different. This observation motivates our
 303 formulation of a general approach to optimize for a kit of parts
 304 that can be customized towards specific classes of bending-active
 305 structures.

306 Our algorithm takes as input a set of existing design instances,
 307 given by the individual geometries of all elastic elements in their
 308 rest state, and corresponding assembly graphs that define the
 309 connectivity of elements in each final structure. The goal is then to
 310 optimize for a sparse kit of parts, that is, to find the optimal geome-
 311 try of each part as well as an assignment function that determines
 312 which element in each input design will be realized by which part.
 313 Such a kit of parts will be effective, if the number of parts is signifi-
 314 cantly smaller than the number of elements, while at the same time
 315 enabling faithful reproduction of the input designs.

316 We first define a template optimization problem in Section 4. Our
 317 formulation abstracts from class-specific implementation details
 318 and focuses on the core objectives that are common across different
 319 classes of bending-active structures. Specifically, we show in Sec-
 320 tion 5 how the combinatorial problem of assigning parts to elements
 321 can be solved with a continuous relaxation that allows integrating
 322 a physics-based simulation to track equilibrium states of the given
 323 input designs. We then illustrate in Section 6 how this template
 324 optimization can be overloaded with specific objectives for three
 325 concrete bending-active structures: (i) umbrella meshes, (ii) orthogon-
 326 al grids, and (iii) C-shells. Implementation aspects of the numerical
 327 optimization are discussed in Section 7 with more details provided
 328 in the supplemental material.

329 We show in Section 8 how our algorithm enables users to analyze
 330 different design choices for the optimization of a kit of parts. This
 331 helps to find the most appropriate trade-off between the complexity
 332 of the kit of parts and the deviation to the input designs.

4 PROBLEM STATEMENT

333 In this section we introduce terminology and formulate the general
 334 problem of optimizing a kit of parts for bending-active structures.

335 We assume as input a set S_1, S_2, \dots of bending-active structures
 336 that represent the variability in designs that should be realizable by
 337 the kit of parts. Each structure S_k is represented by a graph \mathcal{G} whose

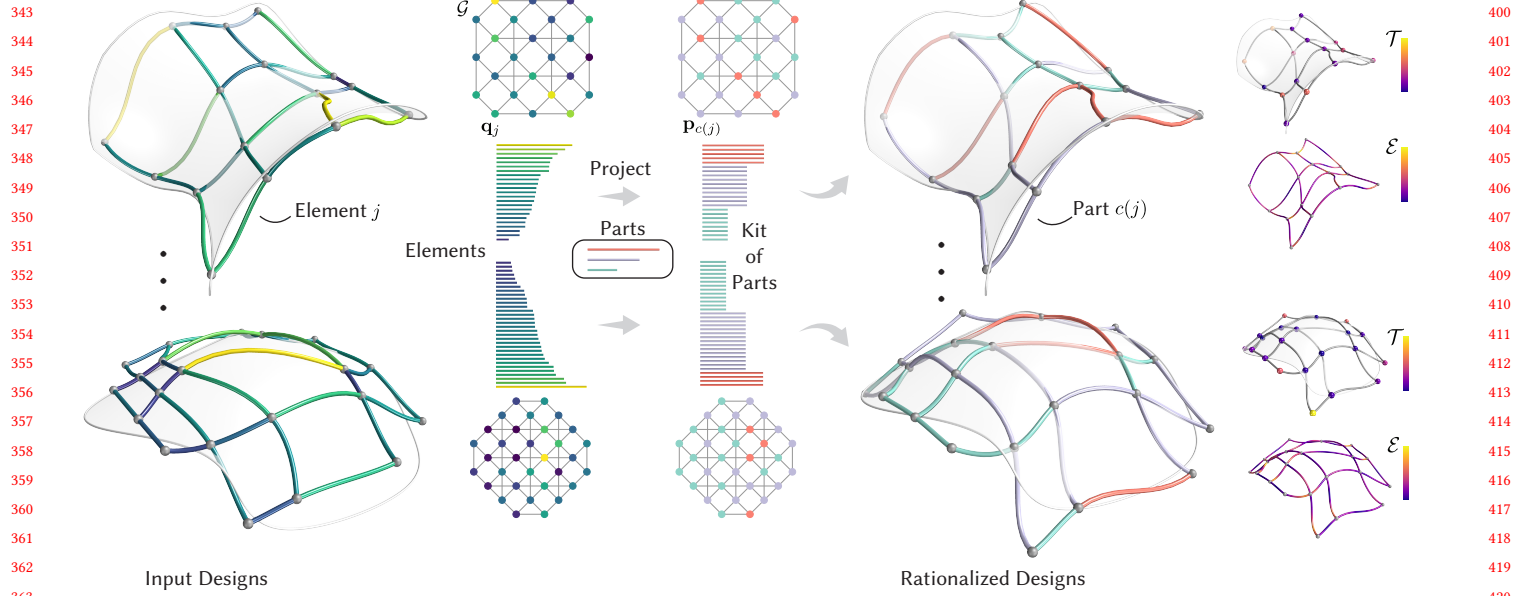


Fig. 3. Rationalization of a bending-active structure using a kit of parts: Graph G defines the assembly connectivity of the design with nodes representing constituent elements/beams. Projecting these designs onto a kit of parts replaces each element j with parameters q_j by a part $c(j)$ from the part set with parameters $p_{c(j)}$. Here c represents the assignment function from elements to parts. The part set and the subsequent kit of parts are computed through an optimization that minimizes and objective comprising target fitting \mathcal{T} and elastic energy \mathcal{E} of the equilibrium state.

nodes denote the elastic elements of the structure that are joined according to the connectivity defined by the graph edges. Each node has attributes $q_j \in \mathbb{R}^d$, a set of continuous parameters that define the element geometry. For example, q_j could denote the length and width of a straight beam and the location of rotational joints along the beam. For ease of notation, we accumulate all element parameters in a vector $q = (q_1, \dots, q_n)$ where n is the total number of elements across all input designs.

4.1 Equilibrium Computation

To simulate the equilibrium of a structure S_k , we convert the corresponding element parameters into a discrete representation suitable for simulation. In our case, we model elastic beams using the discrete elastic rod model introduced by Bergou and colleagues [2010; 2008]. Each beam is sampled with a polyline. The rest variables of the structure are then the lengths and angles of these polylines that we collect in a vector r . The simulation variables representing a deformed state of the design, i.e., the nodal positions and local frames of all discrete elastic rods, are collected in a vector x . The elastic energy of the deformation is defined as $\mathcal{E}(x, r)$ and combines stretching, bending, and twisting terms as proposed in [Bergou et al. 2010].

The deformed state of S_k at equilibrium is the solution x^* of a constrained minimization problem. The optimization objective combines the elastic deformation energy $\mathcal{E}(x, r)$ with external deployment forces modeled by an energy term $\mathcal{D}(x)$. We also integrate Dirichlet constraints to fix a certain subset of the deformed state variables $x_f \subset x$ to user-specified target values x_f^{tgt} , allowing

pinning vertices to fixed positions or simulating deployment. We aggregate the rest variables with the fixed variables in a vector of design variables d . We define the equilibrium state x^* as a function of design variables d as

$$\begin{aligned} x^*(d) := \operatorname{argmin}_x \mathcal{E}(x, r) + \mathcal{D}(x) \\ \text{s.t. } x_f = x_f^{tgt}. \end{aligned} \quad (1)$$

4.2 Kit of Parts Objective

A kit of parts is an ensemble of m parts $p := (p_1, \dots, p_m)$, where $p_i \in \mathbb{R}^d$ define the parts' geometry analogous, but potentially different to the parameterization used for elements of the input designs.

To realize the structures S_k with the kit of parts p , we define an assignment function $c : [1, n] \rightarrow [1, m]$ that indicates which part of p is assigned to which element in q . These assignments are aggregated over all structures in a vector $c = (c(1), \dots, c(n))$. The assignment process is described in more detail in Section 5.2. Figure 3 illustrates q , p , and c for a simple bending-active system. See also Figure 6 and Section 6 for the specific classes we consider below.

The optimization aims to compute the part parameters of p with $m \ll n$ and the corresponding assignment c such that element q_j can be rationalized as an instance of part $p_{c(j)}$. This projection onto the kit of parts inevitably incurs a deviation in the resulting equilibrium shapes from the input designs. Our goal is to reduce this discrepancy to a minimum while retaining a low elastic energy of the system. We thus formulate a design preservation energy as a

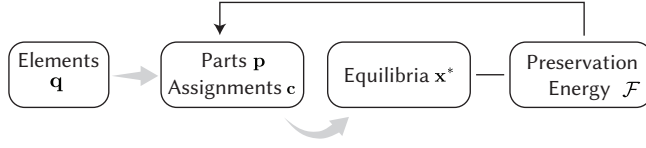


Fig. 4. Optimization flow for the original kit of parts problem. The objective is to find the optimal part parameters p and assignments c that minimize the design preservation energy \mathcal{F} across all designs.

function of (\mathbf{x}, \mathbf{r}) as,

$$\mathcal{F}(\mathbf{x}, \mathbf{r}) = \mathcal{T}(\mathbf{x}) + \mathcal{E}(\mathbf{x}, \mathbf{r}), \quad (2)$$

where \mathcal{T} is a non-dimensionalized target fitting term measuring the distance of the deformed state \mathbf{x} to a given target surface, and \mathcal{E} is the non-dimensionalized elastic energy of \mathbf{x} . We discuss how \mathcal{F} can be adapted to different systems in Section 6.

Once a design S_k is rationalized using the kit of parts p , its rest variables \mathbf{r}_k and design variables \mathbf{d}_k are a function of the part parameters p and the assignment c . As a consequence, the equilibrium state $\mathbf{x}_k^*(\mathbf{d}_k)$ is a function of (p, c) as well. We therefore formulate the objective function for the kit of parts optimization as the sum of the design preservation energies across all designs:

$$\mathcal{J}(p, c) = \sum_k \mathcal{F}\left(\mathbf{x}_k^*(p, c), \mathbf{r}_k(p, c)\right). \quad (3)$$

Figure 4 illustrates the optimization problem. Optionally, weights can be assigned to indicate the relative importance of each design and re-formulate the objective as a weighted sum of design preservation energies.

5 KIT OF PARTS OPTIMIZATION

The equilibrium state \mathbf{x}^* in Equation (3) is sensitive to changes in the kit-of-parts variables (p, c) . A change in the assignment function can lead to a large jump in the equilibrium state \mathbf{x}^* and subsequently the design preservation energy \mathcal{J} . In addition, the space of assignments c grows exponentially with m , making an exhaustive search over the m^n possibilities intractable. The projection of elements q onto parts p in the context of bending-active structures is challenging and can result in buckled equilibrium states. **The projection of elements q onto parts p in the context of bending-active structures is challenging and can result in buckled equilibrium states.** We discuss more about buckling issues in Section 8 and Figure 11 illustrates how our approach mitigates them.

5.1 Projection-Relaxed Problem

We address the forementioned challenges by formulating a relaxation of the problem of minimizing Equation (3) to a tractable continuous optimization. This relaxation is achieved by tracking auxiliary continuous variables \tilde{q} of the elements in the simulation.

We define the kit-of-parts parameters (p, c) as dependent variables of \tilde{q} and introduce a projection energy \mathcal{P} to bind the auxiliary variables \tilde{q} to the parts and assignment variables (p, c) . The rest variables \mathbf{r}_k and the equilibrium state $\mathbf{x}_k^*(\mathbf{r}_k)$ of design S_k are defined as

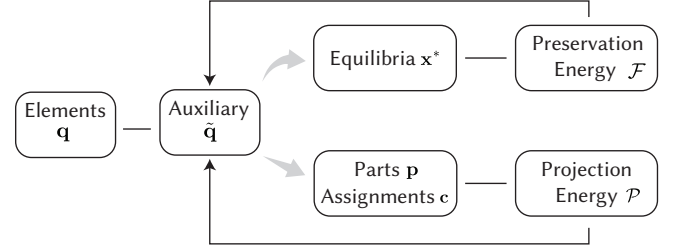


Fig. 5. Optimization flow for the relaxed problem. The relaxation enables a fully differentiable optimization that can be seamlessly combined with a physics-based simulation. **The elements q and parts p are illustrated in Figure 6. Figure 7 visualizes the part assignments c and equilibria x^* along with the energies \mathcal{F} and \mathcal{P} .**

functions of \tilde{q} . The new objective is then written as a function of \tilde{q} :

$$\mathcal{J}(\tilde{q}) = \sum_k \mathcal{F}\left(\mathbf{x}_k^*(\tilde{q}), \mathbf{r}_k(\tilde{q})\right) + \mathcal{P}(\tilde{q}). \quad (4)$$

As opposed to the former objective of Equation 3, part parameters p and part assignments c are dependent variables of \tilde{q} and are updated in the optimization loop. The relaxed formulation defines the equilibrium simulation as a function of the continuous variables \tilde{q} and makes \mathcal{J} robust to large jumps due to changes in the assignment function. The optimization flow is illustrated in Figure 5. The various terms in $\mathcal{J}(\tilde{q})$ specific to our bending-active systems are defined in Section 6 and illustrated in Figure 7 on a single design instance for each system.

5.2 Projection Energy

To define \mathcal{P} , we first introduce a non-dimensionalized part-element projection energy $\rho : \mathbb{R}^d \times \mathbb{R}^d \rightarrow \mathbb{R}_+$. A low value of $\rho(p_i, \tilde{q}_j)$ indicates higher similarity between an element j and a part i . For independent parts p , assignment c , and elements \tilde{q} , the projection energy $\tilde{\mathcal{P}}(p, c, \tilde{q})$ is aggregated over all elements as,

$$\tilde{\mathcal{P}}(p, c, \tilde{q}) := \frac{w_c}{n} \sum_{j=1}^n \rho(p_{c(j)}, \tilde{q}_j), \quad (5)$$

where the weight w_c controls the relative importance given to the projection energy term during optimization. Minimizing $\tilde{\mathcal{P}}$ ensures that the elements are well represented by the parts they have been assigned.

The projection energy $\mathcal{P}(\tilde{q})$ from Equation (4) is then obtained as a minimum over all possible parts and assignments for a given set of elements \tilde{q} ,

$$\mathcal{P}(\tilde{q}) := \min_{p, c} \tilde{\mathcal{P}}(p, c, \tilde{q}). \quad (6)$$

We minimize $\tilde{\mathcal{P}}$ in an alternating fashion over assignment and part updates.

Updates. The assignment c , or the function c , is updated by keeping p fixed and solving for the optimal assignment,

$$c(j) := \operatorname{argmin}_i \rho(p_i, \tilde{q}_j). \quad (7)$$

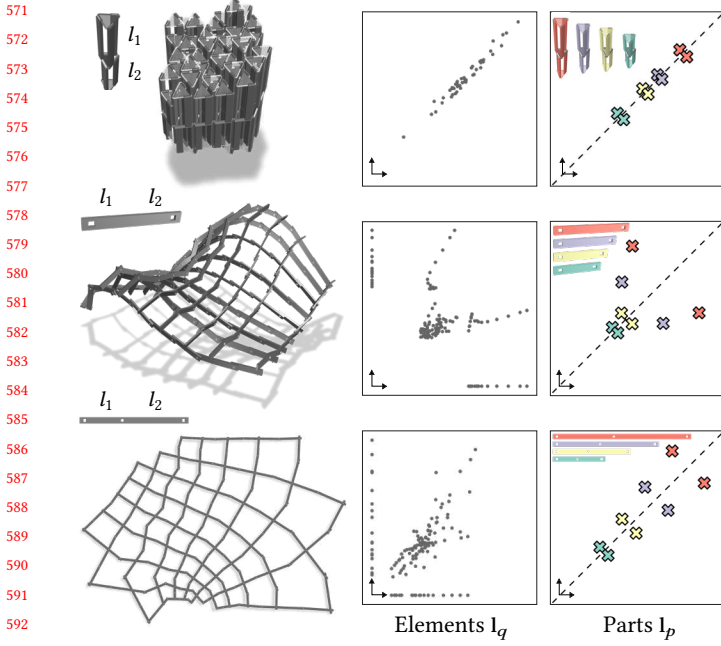


Fig. 6. Elements, parts and assembly states of the three classes of bending active structures that we consider. From top to bottom: Umbrella Meshes, orthogonal grids, C-shells. The plots on the right illustrate the distribution of parameters in input models compared to an optimized kit of parts, where element symmetries can be exploited to further reduce the number of parts.

The parts p are then updated by keeping c fixed and solving for the optimal parts,

$$p_i(\tilde{q}) := \operatorname{argmin}_{y \in \mathbb{R}^d} \sum_{j \in c^{-1}(\{i\})} \rho(y, \tilde{q}_j), \quad (8)$$

where $c^{-1}(\{i\})$ is the set of elements currently assigned to part i . In all of our examples, the update step in Equation (8) can be solved analytically and efficiently differentiated through. The alternating updates are repeated until convergence for every evaluation of $\mathcal{P}(\tilde{q})$. Note that when ρ is the squared L^2 distance, the update rules are equivalent to the k -means clustering algorithm [MacQueen et al. 1967].

Initialization. The alternating update scheme to compute $\mathcal{P}(\tilde{q})$ requires an initial guess for (p, c) . Our initialization is inspired by the k -means++ algorithm [Arthur et al. 2007], so that parts are as spread out over the set of elements as possible. A first element is chosen uniformly at random and assigned to the first part p_1 . A new element \tilde{q}_j is chosen at random among the remaining elements according to a probability proportional to the squared distance $\min_i \rho(p_i, \tilde{q}_j)^2$, where i spans the initialized parts and j indexes the remaining unassigned elements. The chosen element j is then assigned to part i and i is added to the set of initialized parts. This process is repeated until m parts have been constructed. We observe in Figure 7 (left) that such a process allows the parts to span the element space well.

6 SPECIALIZATION TO BENDING-ACTIVE SYSTEMS

We specialize our general computational pipeline to optimize a kit of parts for the chosen bending-active systems: Umbrella Meshes [Ren et al. 2022], Orthogonal Grids, and C-shells [Becker et al. 2023]. Physics-based simulations of the involved bending-active structures are based on the methods presented in the respective papers which have been validated by fabricating prototypes.

We formulate the objective from Equation (3) specific to these three systems. In particular, we define the elements and parts parameterizations, the deployment process, and the element-to-part projection energy. The datasets of shapes for all systems are shown in the supplemental material.

6.1 Umbrella Meshes

Umbrella Meshes are composed of modular volumetric scissor linkages, coined *umbrella cells*. Each umbrella cell deploys from a compact vertical configuration to a flat expanded state whose footprint depends on the height of the cell. When umbrella cells of different heights are assembled together and deployed, metric frustration due to expansion incompatibilities causes the structure to deform into a doubly-curved bending-active surface structure. The top corner of Figure 6 illustrates the elements that make up an umbrella cell, which can be rationalized into a kit of parts for subsequent assembly and deployment. The plates, X-joints and T-joints are identical across all the designs.

Preservation Energy. Each umbrella cell is defined in its rest state by the lengths of the arms connected to the top plate (top heights) and the lengths of the arms connected to the bottom plate (bottom heights). [Ren et al. 2022] explain how different top and bottom heights lead to programming mean curvature in the deployed state. The rest variables r are defined as the aggregation of these lengths. The design variables d may also include pinned vertices at the boundary as for model 2 in Figure 11. The structure is deployed in a similar strategy to the one described in [Ren et al. 2022]: top and bottom plates are brought together through a linear actuator and rigid motions are pinned using small surface attraction forces when there are no boundary constraints. These additional conservative forces responsible for deployment are modeled by the energy term \mathcal{D} in Equation (1). The resulting deployed state x^* is then used to evaluate the objective \mathcal{J} in Equation (4).

Projection Energy. Each umbrella unit/part, is parameterized by the length of the arms of the top plate and the bottom plate, $l_q \in \mathbb{R}_+^2$. Naturally, we define parts as two lengths $l_p \in \mathbb{R}_+^2$. Parts can be used as is or in a mirrored configuration, which is illustrated by the mirror symmetry about the bisector of the first quadrant in Figure 6 (top right). The projection energy between elements and parts is defined as the squared L^2 norm of the difference between the two lengths in both part configurations,

$$\rho(l_p, l_q) = \frac{1}{2l_\rho} \min \left(\|l_p - l_q\|_2^2, \|\text{flip}(l_p) - l_q\|_2^2 \right), \quad (9)$$

where $\text{flip}(p_i)$ flips the lengths of the part p_i , and l_ρ is chosen as the median of the arm lengths across the input designs. In this case, the update rule in Equation (8) can be solved analytically by sorting the assigned elements' lengths and taking the mean. Note that the

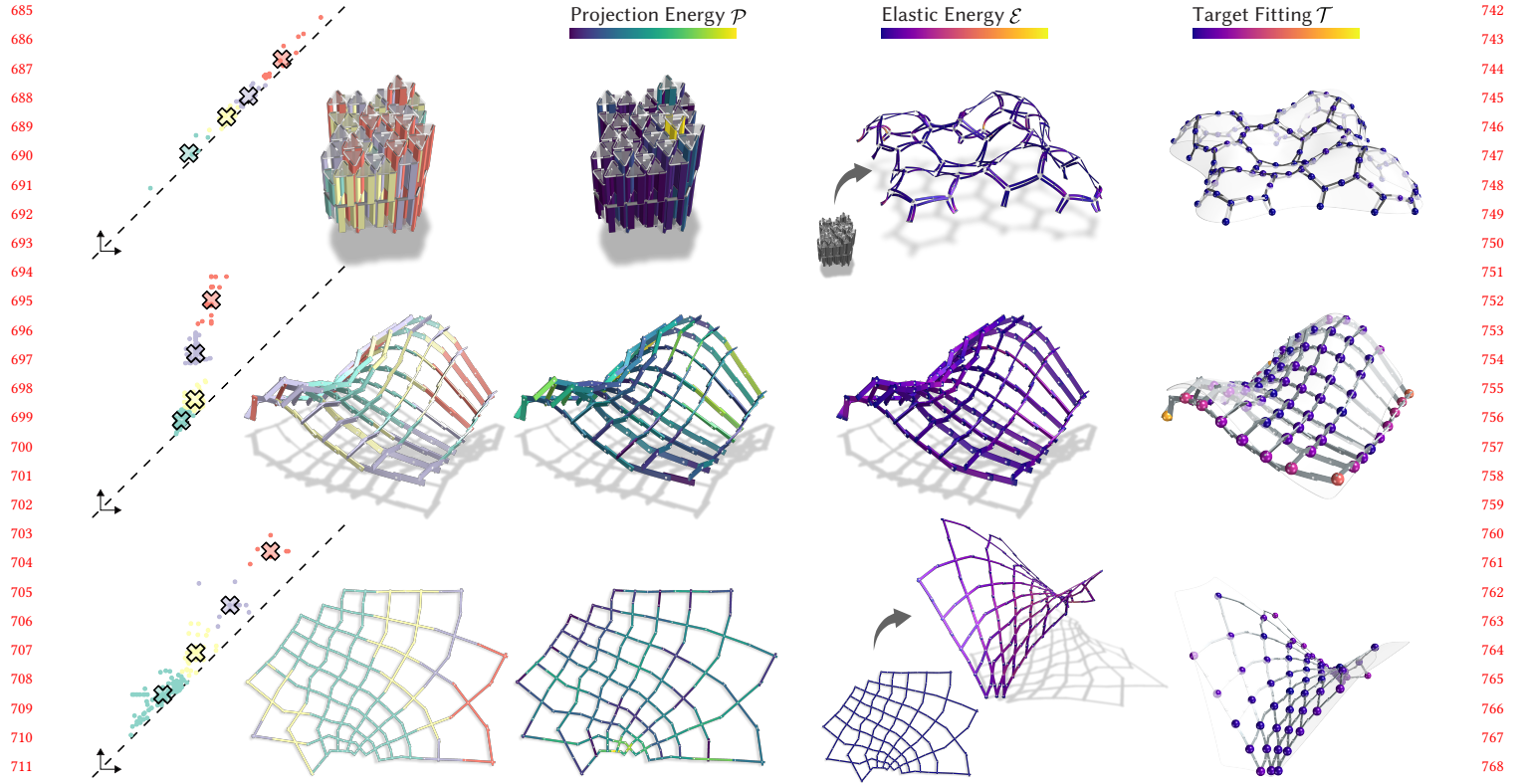


Fig. 7. Optimization objectives in the relaxed problem: For a given input design, the objective function \mathcal{J} is composed of the design preservation energy \mathcal{F} ($= \mathcal{T} + \mathcal{E}$) and the projection energy \mathcal{P} . The plots on the left show distributions of element parameters \bar{q} and the optimal part assignments (p, c) minimizing the projection energy \mathcal{P} . The dots and crosses represent \bar{q} and p as defined in Figure 6. The subsequent columns illustrate each of the terms in \mathcal{J} for the three classes of bending-active structures.

sorting indices need to be stored to ensure the correct assignment of the parts to the elements.

6.2 Orthogonal Grids

Orthogonal grids are bending-active structures composed of elastic lamellas attached at the crossings. The lamellas are oriented such that their strong axis is orthogonal to the input design surface. C-meshes [Liu et al. 2023b] shown in Figure 2 are a special case of orthogonal grids that further imposes the structure to be collapsible into a flat state. In general, orthogonal grids require curved elements to best approximate the underlying target surface. We rationalize the curved rods as piecewise straight beams rigidly connected at their corners. Exactly one corner is allowed between two neighboring joints along each rod, to spatially separate inner- and inter-rod connections.

Preservation Energy. The design state \mathbf{d} of an orthogonal grid comprises rod segment rest lengths together forming the rest variables vector \mathbf{r} , and corner angles. Inter-rod connections are simulated using rotational joints, effectively constraining the intersection point of two rods while allowing rotation. Corners, or inner-rod connections, are simulated as rigid joints with the opening angle between

two rod segments treated as a fixed variable. The corner angles form the set of fixed simulation variables \mathbf{x}_f (Dirichlet constraints) of the equilibrium problem in Equation (1). We rule out rigid motions of the structures during simulation using the same strategy as in Umbrella Meshes.

Projection Energy. Each straight element is parameterized by the distance from the first corner joint to the rotational joint and the distance from the rotational joint to the second corner as shown in Figure 6 (left). The order of the corners is given by following the curves in the original design. Boundary elements are distinguished from inner elements as they have only one corner joint, and are defined by a single length.

We consequently define each part as two lengths $\mathbf{l}_p \in \mathbb{R}_+^2$. Similar to parts in Umbrella Meshes, parts can be used as is or mirrored. The projection energy is defined equivalently to the Umbrella Meshes case, and the parts update rule is solved similarly using the sort strategy. We use the median of the rod lengths across the input designs as the reference length l_p in Equation (9).

To ease the assembly process, corner angles are also grouped into their own discrete set of parts. Our kit of parts is then composed of two types of parts: straight beams (linear parts) and corner angles (angular parts). The corner angles are parameterized by the angle

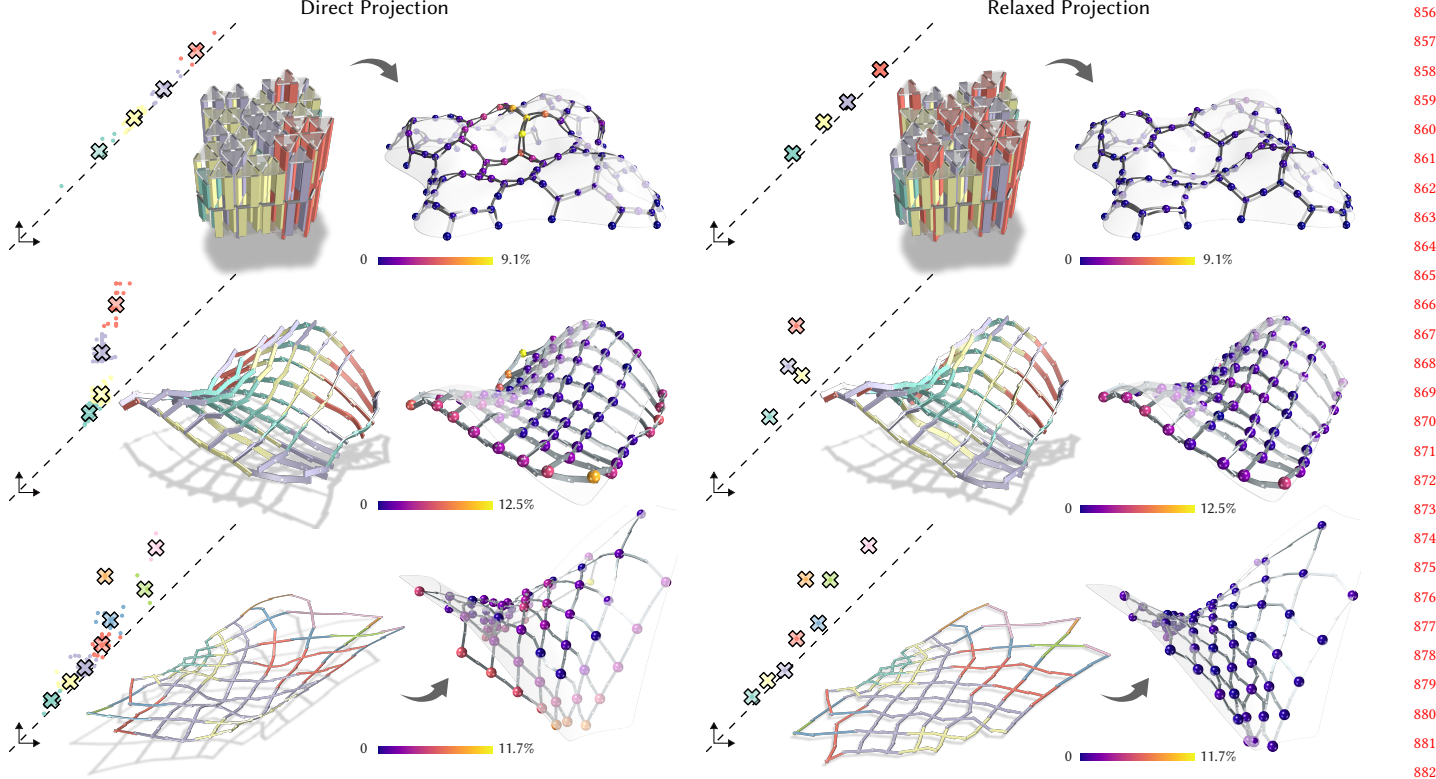


Fig. 8. The parts $p(q)$ and assignment $c(q)$ directly extracted from the original design yields poor preservation of the target shape (left). By re-arranging and collapsing elements around their assigned parts, our relaxed optimization process allows for a better preservation of the initial design (right).

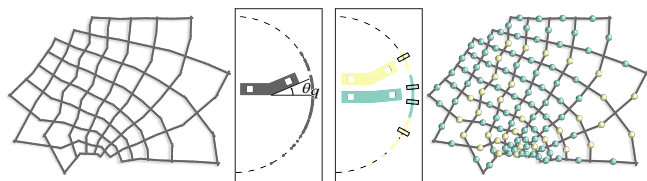


Fig. 9. Angular elements $\theta_q \in [-\pi, \pi]$ are computed at the corners of rationalized C-shells. The angular part is defined by a single angle $\theta_p \in [0, \pi]$ and can be flipped. We represent the angular elements, the 2 parts and their flipped configurations on the unit circle.

between the two straight beams they connect, as shown in Figure 9. Parts are defined subsequently by a single angle $\theta_p \in [0, \pi]$, and can be mirrored during assembly. Our projection energy is then defined as the squared difference between the two unsigned angles $\rho(\theta_p, \theta_q) = \frac{1}{2} (\theta_p - |\theta_q|)^2$. Based on that definition, the update rule in Equation (8) is the average of the assigned elements' unsigned angles.

6.3 C-shells

C-shells are deployable gridshells composed of curved elastic beams connected through rotational joints [Becker et al. 2023]. The assembled state is stress-free by definition and the structure is deployed

via torque actuation, by constraining the average opening angle at the rotational joints. For a completely custom fabricated C-shell tailored to deploy to a specific surface, the curved beams are laser cut precisely following some optimized splines. Similar to Orthogonal Grids, we rationalize each of the curved beams using piecewise straight beams joined at rigid corners. Rotational and corner joints now share the same axis in the rest state.

Preservation Energy. Each rationalized C-shell is defined by the lengths of the straight beams, the corner angles, and the average opening angle of the single-axis rotational joints in the deployed state. These design variables are aggregated in d . Rigid connections at the corners are simulated using Dirichlet constraints in Equation (1). Depending on the values of beam lengths and corner angles, a rationalized C-shell no longer has a guaranteed zero-energy *rest equilibrium state* when assembled. We therefore compute this state x_r^* by solving an equilibrium problem for the assembly configuration. The deployed equilibrium state x_d^* is obtained by further constraining the average opening angle at the rotational joints as described in Becker et al. [2023]. In order to mitigate incompatibilities in the rest state x_r^* and ease assembly, we incorporate the energy of the rest equilibrium state in the preservation energy as

$$\mathcal{F}(x_r, x_d, r) = \mathcal{T}(x_d) + \mathcal{E}(x_d, r) + \mathcal{E}(x_r, r), \quad (10)$$

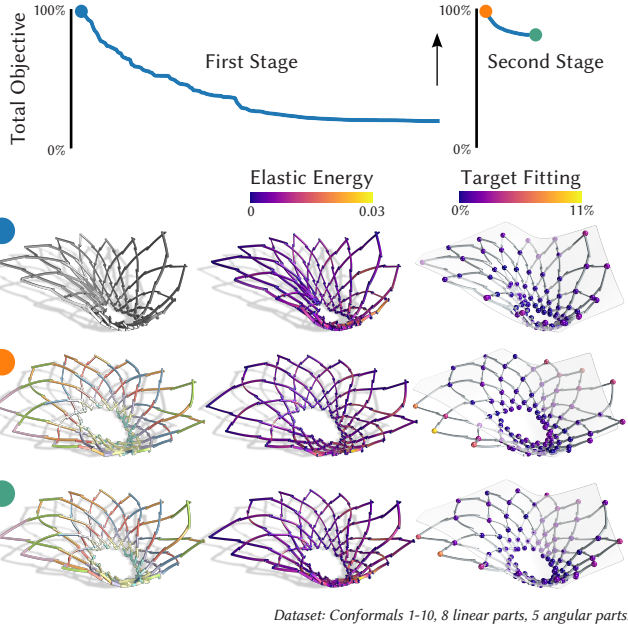


Fig. 10. Our two stage optimization fine tunes designs after first optimizing the relaxed problem. The arrow indicates the projection of the solution of the first stage $\tilde{\mathbf{q}}^*$ onto the part set to obtain $\mathbf{p}(\tilde{\mathbf{q}}^*)$, the initial guess for the second stage. We plot the objective of each stage normalized with respect to the initial value for that stage. The associated rows show the designs at the start, between the two stages, and at the end of the full optimization process.

and we update \mathcal{J} to track both equilibria as

$$\mathcal{J}(\tilde{\mathbf{q}}) = \sum_k \mathcal{F}\left(\mathbf{x}_{r,k}^*(\tilde{\mathbf{q}}), \mathbf{x}_{d,k}^*(\tilde{\mathbf{q}}), \mathbf{r}_k(\tilde{\mathbf{q}})\right) + \mathcal{P}(\tilde{\mathbf{q}}), \quad (11)$$

where k indexes the different designs in the input set.

Projection Energy. We define each linear part as two lengths $\mathbf{l}_p \in \mathbb{R}_+^2$, and each corner angle as a single angle $\theta_p \in [0, \pi]$. The projection energies between elements and parts of the same type, and the parts' update rules are defined identically to the Orthogonal Grids case.

7 TWO-STAGE OPTIMIZATION

We first show a direct rationalization approach in Figure 8 that computes parts \mathbf{p} and assignments \mathbf{c} directly from the input elements \mathbf{q} by minimizing $\tilde{\mathcal{P}}(\mathbf{p}, \mathbf{c}, \mathbf{q})$. This approach does not take the design preservation energy \mathcal{F} into account and can lead to undesired buckling in the output designs. Then, we illustrate the performance of the unrelaxed approach from Section 4 which optimizes the part parameters \mathbf{p} using the assignments from minimizing $\tilde{\mathcal{P}}(\mathbf{p}, \mathbf{c}, \mathbf{q})$ directly. We then compare our relaxed approach in Figure 11. We propose a two-stage optimization approach that first optimizes the relaxed problem and then fine-tunes the parts \mathbf{p} while keeping the assignments \mathbf{c} fixed to minimize the total preservation energy \mathcal{F} . We show the results of our approach in Figure 12.

7.1 First Stage: Relaxation

The original design rationalization problem described in Section 4 is a combinatorial optimization problem, where the number of possible part-to-element assignments grows as m^n . This makes the problem intractable for large elements count n and a non trivial kit of parts i.e., when $m > 1$.

Instead, our relaxation allows leveraging tools from the continuous optimization literature to efficiently solve the constrained minimization problem

$$\tilde{\mathbf{q}}^* := \operatorname{argmin}_{\tilde{\mathbf{q}}} \mathcal{J}(\tilde{\mathbf{q}}), \text{ s.t. } \mathbf{p}_{\min} \leq \tilde{\mathbf{q}} \leq \mathbf{p}_{\max}, \quad (12)$$

where $\tilde{\mathbf{q}}$ now contains all elements of different kinds (linear and angular if applicable), and \mathbf{p}_{\min} and \mathbf{p}_{\max} are (potentially infinite) lower and upper bounds. These are derived from the parts feasibility and fabricability constraints e.g., for the minimum distance between corners and joints for linear parts of rationalized Orthogonal Grids and C-shells. We assume that elements of the same kind share the same bound constraints. In the supplemental material we show that for all the part-element projection energies ρ we use in our experiments, the resulting parts obtained from the optimal elements $\mathbf{p}(\tilde{\mathbf{q}}^*)$ using the part update rule in Equation (8) are *guaranteed* to satisfy the original feasibility constraints. This fact effectively positions our method as a co-rationalization approach providing an end-to-end parametric control over the output designs with respect to the part feasibility constraints.

Figure 11 shows how our projection on to a kit of parts after our first stage relaxation preserves designs better compared to directly solving the original unrelaxed problem. This forms the base for the second stage of our optimization.

7.2 Second Stage: Fixed Assignment Fine-Tuning

The first stage optimization strives to concentrate all the *auxiliary elements* tightly around the *parts* in order to mitigate the discontinuous elements-to-parts conversion. However, the output goal is still a part set, and thus the auxiliary variables need to be converted to the assigned parts. To this end, we perform a second stage of fine-tuning, where we fix the assignment $\mathbf{c}(\tilde{\mathbf{q}}^*)$ and optimize the part parameters starting from $\mathbf{p}(\tilde{\mathbf{q}}^*)$, as

$$\mathbf{p}^* := \operatorname{argmin}_{\mathbf{q}} \mathcal{J}(\mathbf{p}, \mathbf{c}(\tilde{\mathbf{q}}^*)), \text{ s.t. } \mathbf{p}_{\min} \leq \mathbf{p} \leq \mathbf{p}_{\max}. \quad (13)$$

Here \mathbf{p}_{\min} and \mathbf{p}_{\max} are the lower and upper bounds of the parts parameters, and the objective function \mathcal{J} is defined as in Equation (3). The second stage optimization has a very low number of variables compared to the first stage since the assignments are fixed and the part set is sparse. The fine-tuning explores the part space locally within a specific assignment for a local minimizer of the objective function \mathcal{J} . Figure 10 shows the two stage optimization process and visualizes objectives on an associated design instance. The transition between the two stages often leads to a jump in the elastic energy which is mitigated during the second stage. Figure 12 shows the final results of the two stage optimization process for C-shells and Umbrella Meshes and compares them to the input designs as well as a direct rationalization approach.

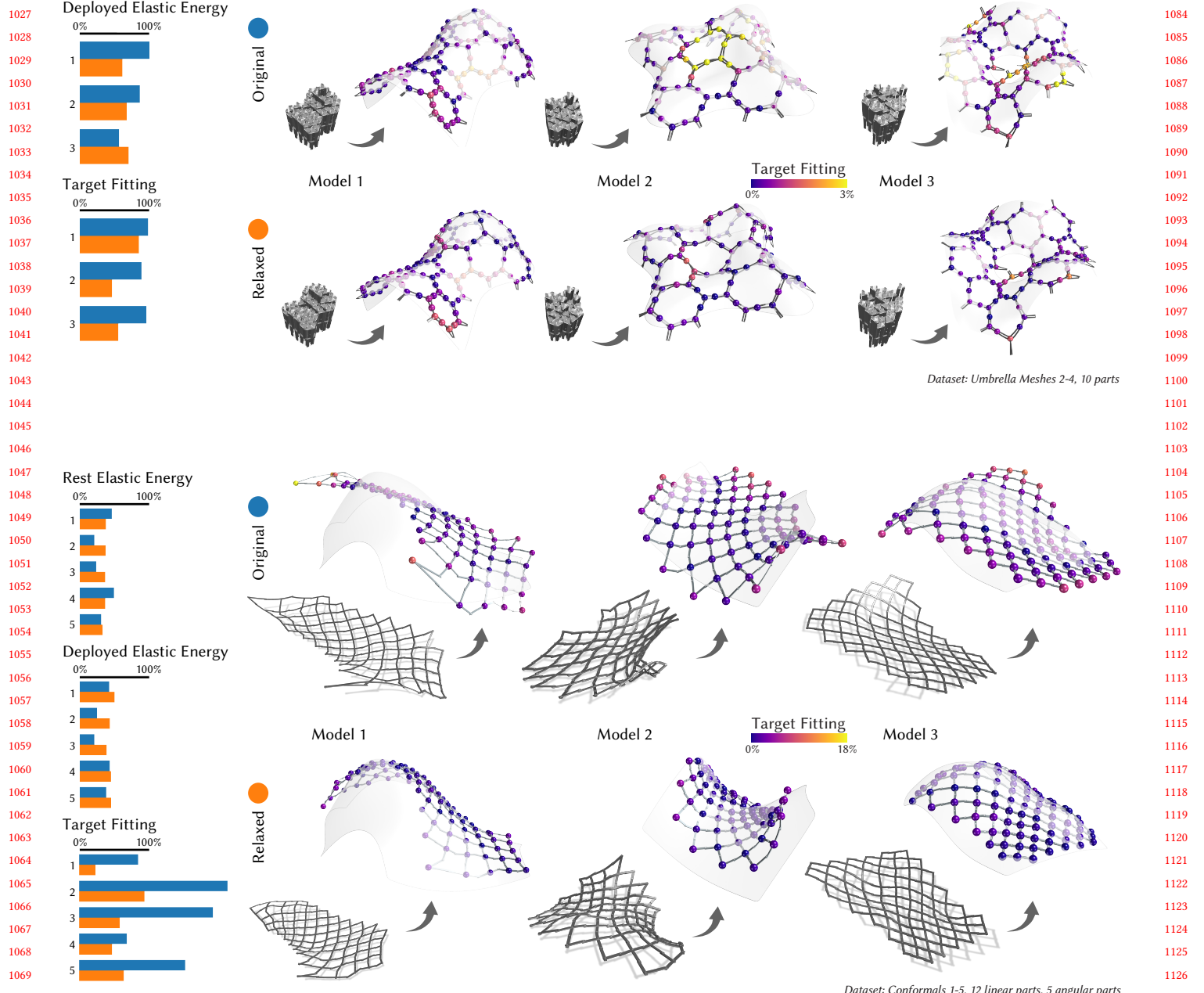


Fig. 11. Solving for the original minimization problem over the parts p in Equation (3) using the original assignments $c(q)$ produces undesired buckling. Our relaxation allows smoothly bringing designs together towards a shared kit of parts. We show designs after the first stage optimization involving the relaxation and project the elements on to the parts at the end of it. We report target fitting as a percentage of each model's bounding box diagonal. We normalize the optimization quantities using the respective initial values for each “projected” design.

7.3 Optimization Algorithm

We solve the optimization problems in Equation (12) and Equation (13) using a trust-region active-set method (Sequential Linear-Quadratic Programming) with a BFGS Hessian approximation [Nocedal and Wright 2006] provided by Knitro [Waltz and Nocedal 2004]. We compute the gradient of the preservation energy \mathcal{F} using

first order adjoint sensitivity analysis. More details on how differentiation with respect to the constrained simulation variables $x_f^{\text{tgt}}(d)$ is performed can be found in the supplemental material.

We use uniform material properties for all the structures in our experiments with Young's modulus E and Poisson's ratio ν set to (1400MPa, 0.35) for Umbrella Meshes, and (2100MPa, 0.35) for

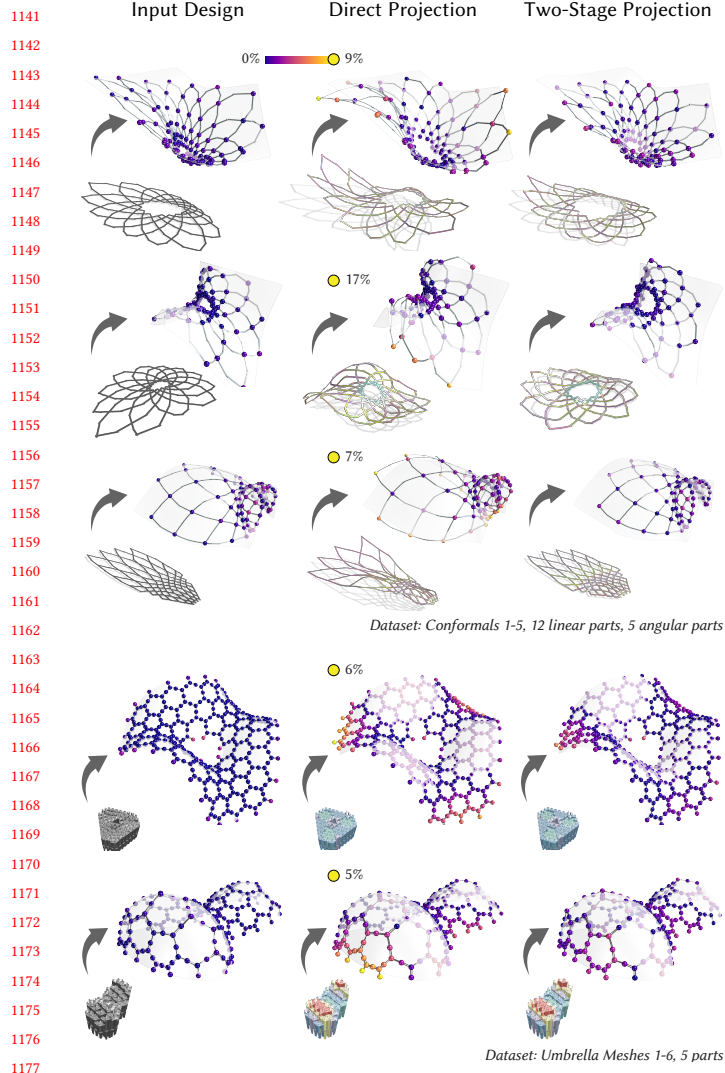


Fig. 12. We show subsets of optimized designs from two different bending-active systems after the two-stage optimization process. The left column shows the input designs, the middle column shows the designs directly projected to the part set. The right column shows the designs after the two-stage optimization process. We report the target fitting as a percentage of each model’s bounding box diagonal.

Orthogonal Grids and C-shells. Our first stage optimization typically converges in 10 minutes to an hour on the examples we show. The second stage optimization runs faster, and typically takes no more than 15 minutes to converge in our experiments.

8 DISCUSSION

Projection onto an Existing Kit of Parts. We demonstrate in Figure 13 how our relaxation approach can be adapted to find the best assembly that approximates an input design using only an existing kit of parts \bar{p} . We jointly optimize the assignment c and the element parameters \tilde{q} for the objective of the relaxed optimization problem

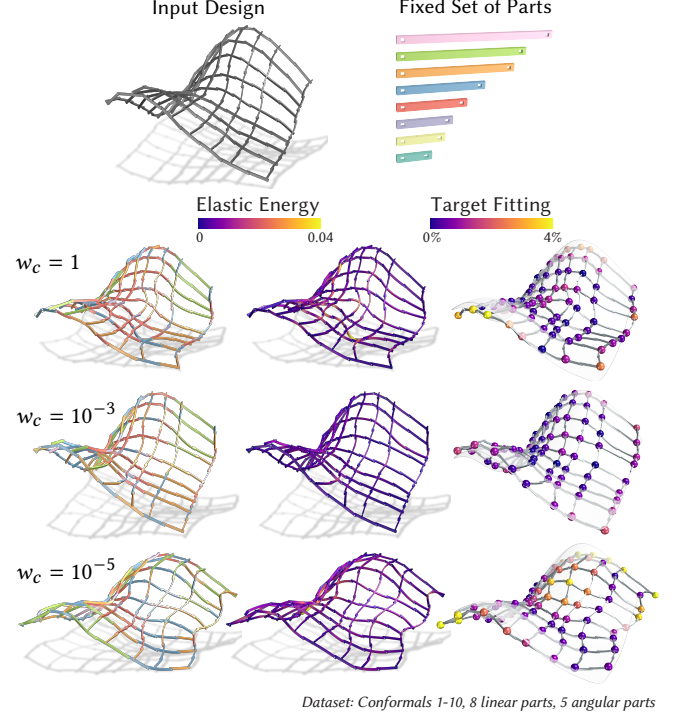


Fig. 13. A new design is projected onto an existing kit of parts. The input design has not been used during the optimization of the kit of parts. Tuning the clustering weight allows recovering a better design.

shown in Equation (4). Since parts are fixed initially, the projection energy \mathcal{P} in Equation (6) becomes by $\min_{\mathbf{c}} \tilde{\mathcal{P}}(\bar{p}, \mathbf{c}, \tilde{\mathbf{q}})$, where $\tilde{\mathcal{P}}$ is defined in Equation (5). As shown in Figure 13, a higher projection energy weight w_c enforces a tighter and faster fit of each element to their initial assignment, preventing them from evolving during the projection operation. Lowering projection energy weight w_c allows smoothly transitioning from the input design to the kit of parts, leading in practice to better assignments. However, if the weight is set too low, the parts are only loosely fit by the elements. The part assignments step may then lead to undesired buckling in the output design, as shown in Figure 13 for $w_c = 10^{-5}$.

Part Reuse. Consider the scenario where we fabricate only as many pieces (instances of parts) as needed such that all the designs can be realized individually using this kit of parts. When we use a small part set, the number of fabricated pieces is low but the design fidelity can suffer due to the limited expressiveness of the parts. On the other hand, a large part set requires more pieces to be fabricated. Our framework can be used to investigate the trade-off between design fidelity and the size of the kit of parts. Figure 14 illustrates the interplay between the kit-of-parts size and the maximum deviation of the design instances from their target surfaces. In the visualized examples of rationalized designs, we observe clear improvement in the target fitting as the number of parts increase, however leading to an increase in the total number of fabricated pieces. Notice that the gain in target fitting diminishes after a certain number of parts (12

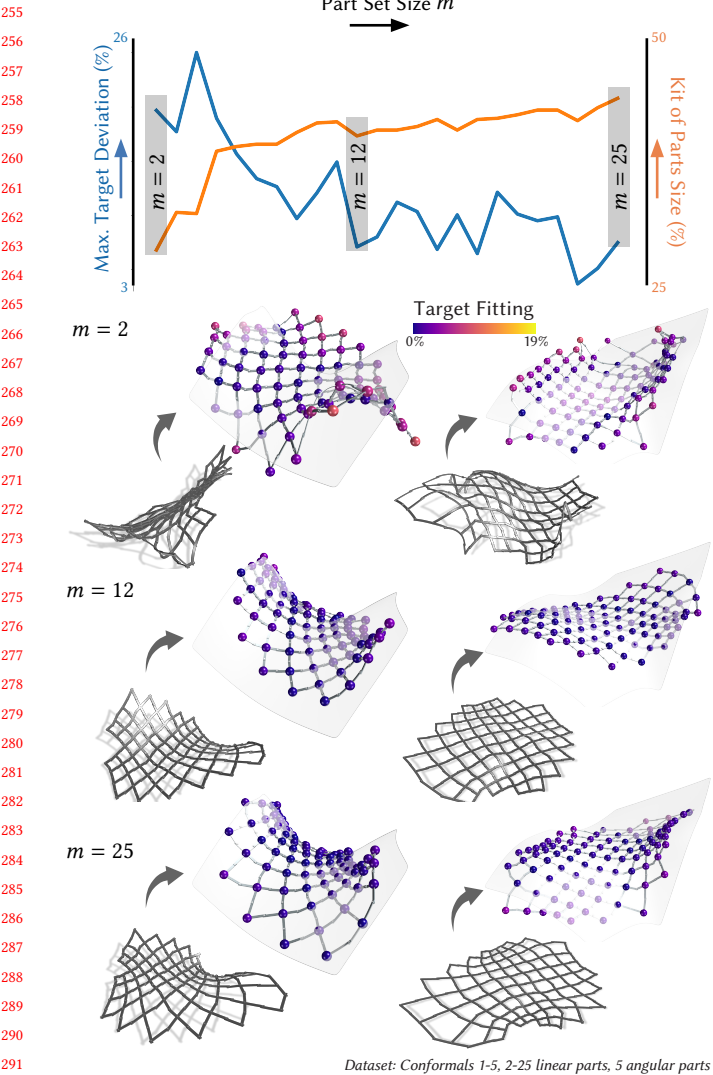


Fig. 14. Increasing the number of distinct parts m trades design fidelity for parts reuse. We jointly optimize 5 designs using the relaxation and show the resulting equilibrium states (of 2 designs) after assigning parts to elements. The kit of parts size is shown as a percentage of the total number of fabricated pieces over the total number of elements in the input designs.

in Figure 14), suggesting that the additional parts do not contribute significantly to the design fidelity. Thus, our framework enables discovery of the most suitable trade-off between design fidelity and fabrication complexity.

With more parts, the likelihood of reusing pieces across different designs decreases. Ideally, we would like to reuse the same pieces across different designs to maximize part reuse. For the five design instances considered in our experiments, we analyze part reuse among different subsets of designs for each part set size. For example, consider the sets of pieces $\mathcal{S}_1, \mathcal{S}_2$ used to assemble two designs respectively. Then the Jaccard similarity $|\mathcal{S}_1 \cap \mathcal{S}_2| / |\mathcal{S}_1 \cup \mathcal{S}_2|$ measures the part reuse between the two designs. Figure 15a shows the

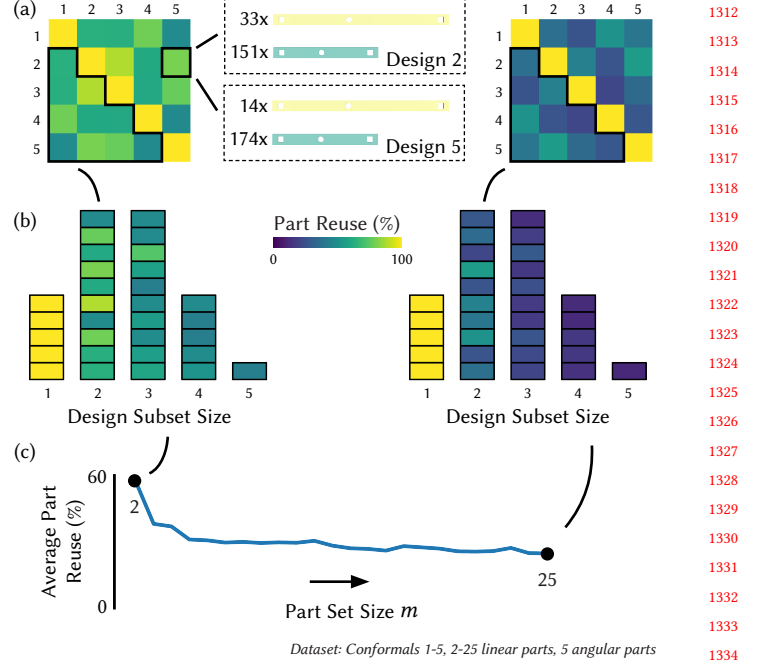


Fig. 15. (a) Pairwise Jaccard similarities between two design instances for two different part set sizes (2, 25). The inset shows the pieces used in two designs (Design 2 and Design 5, with a part set size of 2) explaining the part reuse % in the incidence matrix measuring pairwise part reuse. (b) Generalized subset-wise part reuse. Note that the pairwise similarities correspond to similarities on subsets of cardinality 2. (c) Evolution of average part reuse across all subsets with the part set size.

pairwise Jaccard similarities for the five design instances for two different part set sizes (2, 25). This notion can be extended to more than two designs by considering $|\bigcap_k \mathcal{S}_k| / |\bigcup_k \mathcal{S}_k|$. Visualizing part reuse among different subsets (Figure 15b) can provide insights into disconnected design subsets. A similar analysis can be done over the part subsets to discover disconnected part subsets in the kit of parts. As the number of distinct parts increases, the average part reuse diminishes, as shown in Figure 15c.

Buckling Issues During Projection. Figure 8 shows how a direct projection of elements to parts can lead to undesired buckling even for a single design. Once such a bad assignment is made, optimizing the part parameters doesn't recover the design fidelity as seen in Figure 11. This is because the design objective is a highly non-linear, non-convex function of the rest variables. If elements are projected to parts when the clusters are not *tight* enough, the objective can incur a large jump sometimes manifested as the observed buckling. This problem is pronounced in the case of Umbrella Meshes which have multiple stable configurations owing to a larger design space, making recovery from buckled states hard.

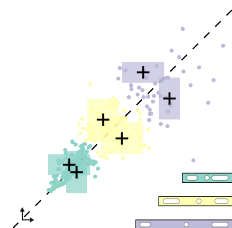
Our relaxation provides a continuous balance between the objectives and brings the elements $\tilde{\mathbf{q}}$ closer to the parts \mathbf{p} first while maintaining the design fidelity. The auxiliary variables $\tilde{\mathbf{q}}$ are then

projected to the parts p at the start of the second stage optimization as described in Section 7.2. Minimizing the relaxation objective $\mathcal{J}(\tilde{q})$ in the first stage brings the elements \tilde{q} *tightly* close to the cluster center parts p controlled by w_c . While this is a significantly better state to project the elements to parts compared to the direct approach, it is unclear how *tight* the clustering should be. Owing to the highly nonlinear design objective, the equilibrium state can show large deviations for small changes in the element size resulting in failure cases like shown in Figure 17. In these scenarios, we increase the projection energy weight w_c before projection to explore better solutions without losing too much design fidelity. When that fails, we understand that the tight cluster of elements cannot be replaced by the cluster center part for this design, and re-initialize the clusters with a larger kit of parts.

Architectural Applications. As discussed in the introduction, bending-active structures are of particular interest in architecture. However, few designs have been realized, partly because of high cost and complexity of custom fabrication. The kit-of-parts approach that we propose can potentially alleviate these issues. In Figure 16 we show some speculative designs realized with our optimized kit of parts to illustrate the potential for applications in architecture.

Part Complexity. In our work, we show a kit-of-parts approach that first discretizes the input bending-active designs into atomic elements and then maps these elements to a part set that is parametrized the same way as each of the elements. We demonstrate results for three bending-active systems using this approach. However, our framework is general and can be extended to include more complex parts that are parametrized differently from the elements. For example, we can include parts that allow continuous adjustments.

The inset shows an example of such more complex parts. Each straight beam has a slit window in which it can be connected to its neighboring elements. With the slits on both ends, the same part could then be used to replace multiple different elements. Similarly, a reconfigurable umbrella part [Kusupati et al. 2023] can be used to replace multiple umbrella cells of different arm lengths that fall in the reconfigurable range. Reconfigurable elements provide additional degrees of freedom to find better solutions for the constrained problem of finding an optimal kit of parts. While complex reconfigurable parts have a greater degree of expressiveness, they also increase the fabrication complexity and can make assembly more difficult. For example, for the slotted parts shown here, parts need to be connected carefully to ensure the slit windows align correctly. In addition, the reconfigurable parts have additional components that can lead to collisions during deployment, or undesired aesthetics. We leave the thorough exploration of these reconfigurable part types for future work.



9 LIMITATIONS AND FUTURE WORK

Buckling Mitigation. While the relaxation approach performs well in our experiments, we cannot currently quantify how close the solution of the relaxed version is to the optimal part set and assignment. Depending on the energy landscape of the equilibrium state that is being tracked, a small perturbation in the element parameters can lead to a significant change in the objective function \mathcal{J} . When the solution from the relaxation problem is such an equilibrium state, we observe a jump (buckling) between the two stages of the optimization, which leads to potentially irrecoverable deployed state. Figure 17 exemplifies this. Since our optimization relies on local sensitivity information we cannot easily predict when such a jump will occur.

Focused Objectives. When optimizing the part geometries, we currently do not directly control re-use efficiency i.e., the number of parts shared among different designs. If structures are to be assembled in sequence, it would be desirable if the next design could re-use as many parts from the previous design as possible to limit the total number of elements that need to be fabricated. A corresponding objective could be integrated into our optimization in future work.

While we currently use an elastic energy term in the design preservation energy to favor low-energy designs, we can also include focused objectives like the maximum stress in the structure. Similarly precise load-bearing behavior could be enforced by including external loads as part of the equilibrium simulation. Incorporating implementations of these specific scenarios into our framework remains a future work.

Input Design Harmonization. Within each dataset, our input structures are designed such that initial elements belong to the same region of the element parameters space. This manual harmonization pre-processing step is necessary to ensure that the downstream optimization converges to parts shared across most designs. Automatically diagnosing the quality of the input designs and providing feedback e.g., in the form of rescaling or topology changes, on how to update the input designs best to make them more compatible with each other could be a valuable addition to our framework. This diagnosis could inform users to amend designs for higher re-use efficiency during early design stages.

Fabrication. The simulation frameworks of the three bending-active systems are based on the discrete elastic rod model [Bergou et al. 2008] which has been extensively validated [Romero et al. 2021]. Umbrella Meshes and C-shells fabricate physical prototypes to validate the simulation results. Our rationalization choices to build these systems with a kit-of-parts do not alter the fabrication process, and our simulation uses the same frameworks used before. However, it is still necessary to validate the rationalized designs with physical prototypes given the sensitivity of the equilibrium states, particularly in the context of bending-active systems. We leave this for future work since it also comes with significant engineering challenges to design an easy assembly/disassembly process. While we focus on fabrication-aware design and optimization of bending-active structures using a kit-of-parts, assembly-aware design is an important aspect that we leave for future work.

1426
1427
1428
1429
1430
1431
1432
1433
1434
1435
1436
1437
1438
1439
1440
1441
1442
1443
1444
1445
1446
1447
1448
1449
1450
1451
1452
1453
1454
1455
1456
1457
1458
1459
1460
1461
1462
1463
1464
1465
1466
1467
1468
1469
1470
1471
1472
1473
1474
1475
1476
1477
1478
1479
1480
1481
1482

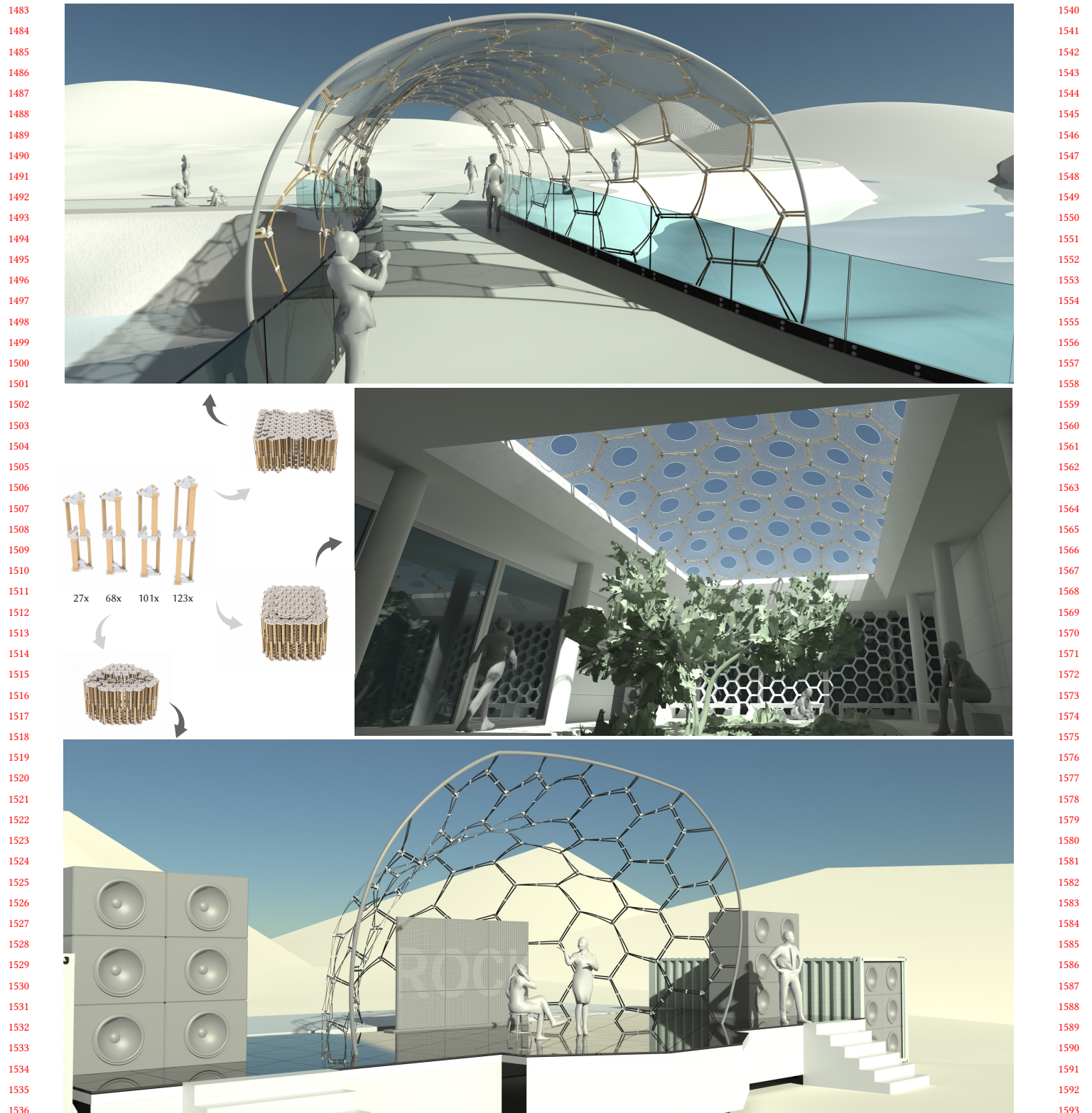


Fig. 16. Architectural applications: Speculative designs realized with an optimized kit of parts.

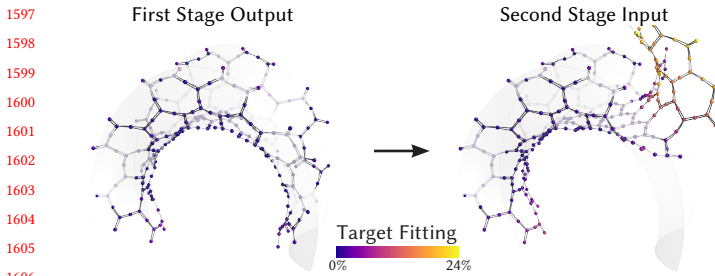


Fig. 17. A failure case of the relaxation approach in between the two stages of the optimization. Slight perturbations in the assembly rest state may result in irrecoverable buckling configurations.

10 CONCLUSION

An optimized kit of parts enables cost-effective and re-use-friendly manufacturing of complex structures. The kit-of-parts approach is particularly attractive for bending-active structures since each part can appear in different configurations i.e., deformed states, of different structures resulting in non-trivial coupling compared to rigid kit-of-parts assemblies. Furthermore, these structures sharing parts are highly sensitive to perturbations of the part geometries due to active bending. Our computational pipeline enables evaluating the trade-offs between the design preservation of input designs and part set size, by leveraging physical simulation of the bending-active equilibria to guide the optimization of the kit of parts.

REFERENCES

- Lara Alegria Mira, Ashley P Thrall, and Niels De Temmerman. 2016. The universal scissor component: optimization of a reconfigurable component for deployable scissor structures. *Engineering optimization* 48, 2 (2016), 317–333.
- Julian M Allwood, Jonathan M Cullen, Mark A Carruth, Daniel R Cooper, Martin McBrien, Rachel L Milford, Muiris C Moynihan, and Alexandra CH Patel. 2012. *Sustainable materials: with both eyes open*. Vol. 2012. UIT Cambridge Limited Cambridge, UK.
- David Arthur, Sergei Vassilivtskii, et al. 2007. k-means++: The advantages of careful seeding. In *Soda*, Vol. 7. 1027–1035.
- Changyeob Baek, Andrew O Sagedam-Furnas, Mohammad K Jawed, and Pedro M Reis. 2018. Form finding in elastic gridshells. *Proceedings of the National Academy of Sciences* 115, 1 (2018), 75–80.
- Paolo Basso, Andrea E Del Grosso, Alberto Pugnale, and Mario Sassone. 2009. Computational morphogenesis in architecture: Cost optimization of free-form grid shells. *Journal of the international association for shell and spatial structures* 50, 3 (2009), 143–150.
- Quentin Becker, Seiichi Suzuki, Yingying Ren, Davide Pellis, Francis Julian Panetta, and Mark Pauly. 2023. C-shells: Deployable Gridshells with Curved Beams. *ACM Transactions on Graphics* 42, 6 (2023), 1–17.
- Miklós Bergou, Basile Audoly, Etienne Vouga, Max Wardetzky, and Eitan Grinspun. 2010. Discrete viscous threads. *ACM Transactions on graphics (TOG)* 29, 4 (2010), 1–10.
- Miklós Bergou, Max Wardetzky, Stephen Robinson, Basile Audoly, and Eitan Grinspun. 2008. Discrete elastic rods. In *ACM SIGGRAPH 2008 papers*. 1–12.
- Jan Brüttig, Gennaro Senatore, and Corentin Fivet. 2021. Design and fabrication of a reusable kit of parts for diverse structures. *Automation in Construction* 125 (2021), 103614.
- Steinar Hillersøy Dyvik, Bendik Manum, and Anders Rønnquist. 2021. Gridshells in recent research—a systematic mapping study. *Applied Sciences* 11, 24 (2021), 11731.
- Michael Eigensatz, Mario Deuss, Alexander Schiffner, Martin Kilian, Niloy J Mitra, Helmut Pottmann, and Mark Pauly. 2010. Case studies in cost-optimized paneling of architectural freeform surfaces. In *Advances in architectural geometry 2010*. Springer, 49–72.
- Corentin Fivet and Jan Brüttig. 2020. Nothing is lost, nothing is created, everything is reused: structural design for a circular economy. *The Structural Engineer* 98, 1 (2020), 74–81.
- Chi-Wing Fu, Chi-Fu Lai, Ying He, and Daniel Cohen-Or. 2010. K-set tilable surfaces. *ACM transactions on graphics (TOG)* 29, 4 (2010), 1–6.
- Grégoire Gaudreault and Andrei Nejur. 2023. Heteromorph: Temporary shelters made of reclaimed heterogeneous materials. 59–68. <https://doi.org/10.52842/conf.ecaade.2023.2059>
- A Scott Howe, Isamu Ishii, and Tomohiro Yoshida. 1999. Kit-of-parts: A review of object-oriented construction techniques. In *ISARC’99: international symposium on automation and robotics in construction (Madrid, 22–24 September 1999)*. 165–171.
- Yijiang Huang, Latifa Alkhayat, Catherine De Wolf, and Caitlin Mueller. 2021. Algorithmic circular design with reused structural elements: method and tool. In *Proceedings of the International fib Symposium on the Conceptual Design of Structures*, Vol. 55. Fédération Internationale du Béton (fib), 457–468.
- Eleni Iacovidou and Phil Purnell. 2016. Mining the physical infrastructure: Opportunities, barriers and interventions in promoting structural components reuse. *Science of the Total Environment* 557 (2016), 791–807.
- Caigui Jiang, Hui Wang, Victor Ceballos Inza, Felix Delling, Florian Rist, Johannes Wallner, and Helmut Pottmann. 2021. Using isometries for computational design and fabrication. *ACM Transactions on Graphics (TOG)* 40, 4 (2021), 1–12.
- Caigui Jiang, Jun Wang, Johannes Wallner, and Helmut Pottmann. 2014. Freeform honeycomb structures. In *Computer Graphics Forum*, Vol. 33. Wiley Online Library, 185–194.
- Uday Kusupati, Florin Isvoranu, Seiichi Suzuki, and Mark Pauly. 2023. RUM: Reconfigurable Umbrella Mesh. *Advances in Architectural Geometry 2023* (2023), 474.
- Riccardo La Magna. 2017. *Bending-Active Plates: Strategies for the Induction of Curvature through the Means of Elastic Bending of Plate-based Structures*. Universität Stuttgart Inst. f. Tragkonstr.
- Julian Lienhard. 2014. *Bending-Active Structures: Form-finding Strategies Using Elastic Deformation in Static and Kinetic Systems and the Structural Potentials Therein*. Universität Stuttgart Inst. f. Tragkonstr.
- Julian Lienhard, Holger Alpermann, Christoph Gengnagel, and Jan Knippers. 2013. Active Bending, a Review on Structures where Bending is Used as a Self-Formation Process. *International Journal of Space Structures* 28, 3–4 (2013), 187–196. <https://doi.org/10.1260/0266-3511.28.3-4.187> arXiv:<https://doi.org/10.1260/0266-3511.28.3-4.187>
- Daoming Liu, Davide Pellis, Yu-Chou Chiang, Florian Rist, Johannes Wallner, and Helmut Pottmann. 2023b. Deployable strip structures. *ACM Trans. Graph* 42, 4 (2023).
- Yuanpeng Liu, Ting-Uei Lee, Antioopi Koronaki, Nico Pietroni, and Yi Min Xie. 2023a. Reducing the number of different nodes in space frame structures through clustering and optimization. *Engineering Structures* 284 (2023), 116016.
- Yizhe Liu, Fei Pan, Bin Ding, Yilong Zhu, Kuijian Yang, and Yuli Chen. 2022. Multistable shape-reconfigurable metawire in 3D space. *Extreme Mechanics Letters* 50 (2022), 101535.
- Zhong-Yuan Liu, Zhan Zhang, Di Zhang, Chunyang Ye, Ligang Liu, and Xiao-Ming Fu. 2021. Modeling and fabrication with specified discrete equivalence classes. *ACM Trans. Graph.* 40, 4, Article 41 (jul 2021), 12 pages. <https://doi.org/10.1145/3450626.3459843>
- Hongjia Lu and Yi Min Xie. 2023. Reducing the number of different members in truss layout optimization. *Structural and Multidisciplinary Optimization* 66, 3 (2023), 52.
- Sheng-Jie Luo, Yonghao Yue, Chun-Kai Huang, Yu-Huan Chung, Sei Imai, Tomoyuki Nishita, and Bing-Yu Chen. 2015. Legolization: Optimizing lego designs. *ACM Transactions on Graphics (TOG)* 34, 6 (2015), 1–12.
- James MacQueen et al. 1967. Some methods for classification and analysis of multivariate observations. In *Proceedings of the fifth Berkeley symposium on mathematical statistics and probability*, Vol. 1. Oakland, CA, USA, 281–297.
- Iason Manolas, Francesco Laccone, Gianmario Cherchi, Luigi Malomo, Paolo Cignoni, et al. 2022. A Computational Tool for the Analysis of 3D Bending-active Structures Based on the Dynamic Relaxation Method,. In *STAG*. 1–9.
- Romain Mesnil, Takara Muto, Krittika Walia, Cyril Doutre, and Olivier Baverel. 2023. *Design and Fabrication of a Pseudo-Geodesic Gridshell*. De Gruyter, Berlin, Boston, 83–96. <https://doi.org/doi:10.1515/978311162683-007>
- Jorge Nocedal and Stephen Wright. 2006. *Numerical optimization*. Springer Science & Business Media.
- Julian Panetta, Mina Konaković-Luković, Florin Isvoranu, Etienne Bouleau, and Mark Pauly. 2019. X-shells: A new class of deployable beam structures. *ACM Transactions on Graphics (TOG)* 38, 4 (2019), 1–15.
- Stefan Pillwein and Przemysław Musiałski. 2021. Generalized deployable elastic geodesic grids. *ACM Transactions on Graphics (TOG)* 40, 6 (2021), 1–15.
- Yingying Ren, Uday Kusupati, Julian Panetta, Florin Isvoranu, Davide Pellis, Tian Chen, and Mark Pauly. 2022. Umbrella meshes: elastic mechanisms for freeform shape deployment. *ACM Transactions on Graphics* 41, ARTICLE (2022), 1–15.
- Victor Romero, Mickaël Ly, Abdullah Haroon Rasheed, Raphaël Charrodière, Arnaud Lazarus, Sébastien Neukirch, and Florence Bertails-Descoubes. 2021. Physical validation of simulators in Computer Graphics: A new framework dedicated to slender elastic structures and frictional contact. *ACM Transactions on Graphics (TOG)* 40, 4 (2021), 1–19.

1654
1655
1656
1657
1658
1659
1660
1661
1662
1663
1664
1665
1666
1667
1668
1669
1670
1671
1672
1673
1674
1675
1676
1677
1678
1679
1680
1681
1682
1683
1684
1685
1686
1687
1688
1689
1690
1691
1692
1693
1694
1695
1696
1697
1698
1699
1700
1701
1702
1703
1704
1705
1706
1707
1708
1709
1710

- 1711 Eike Schling. 2018. *Repetitive Structures*. Ph.D. Dissertation. Technische Universität
1712 München. <https://mediatum.ub.tum.de/1449869>
- 1713 Eike Schling and Rainer Barthel. 2020. Repetitive structures. In *Impact: Design With
1714 All Senses: Proceedings of the Design Modelling Symposium, Berlin 2019*. Springer,
360–375.
- 1715 Eike Schling, Martin Kilian, Hui Wang, Jonas Schikore, and Helmut Pottmann. 2018.
1716 Design and construction of curved support structures with repetitive parameters.
In *Advances in Architectural Geometry*. [https://api.semanticscholar.org/CorpusID: 54173491](https://api.semanticscholar.org/CorpusID:
1717 54173491)
- 1718 Eike Schling, Hui Wang, Sebastian Hoyer, and Helmut Pottmann. 2022. Designing
asymptotic geodesic hybrid gridshells. *Computer-Aided Design* 152 (2022), 103378.
- 1719 Mayank Singh and Scott Schaefer. 2010. Triangle surfaces with discrete equivalence
1720 classes. In *ACM SIGGRAPH 2010 papers*. 1–7.
- 1721 Caroline St-Hilaire and Andrei Nejur. 2022. WoodN - In search of a constructive system
for a sustainable temporary architecture. 185–194. [https://doi.org/10.52842/conf:ecaade.2022.1.185](https://doi.org/10.52842/conf:
1722 ecaade.2022.1.185)
- 1723 Xavier Tellier. 2022. Bundling elastic gridshells with alignable nets. Part I: Analytical
approach. *Automation in Construction* 141 (2022), 104291.
- 1724
- 1725
- 1726
- 1727
- 1728
- 1729
- 1730
- 1731
- 1732
- 1733
- 1734
- 1735
- 1736
- 1737
- 1738
- 1739
- 1740
- 1741
- 1742
- 1743
- 1744
- 1745
- 1746
- 1747
- 1748
- 1749
- 1750
- 1751
- 1752
- 1753
- 1754
- 1755
- 1756
- 1757
- 1758
- 1759
- 1760
- 1761
- 1762
- 1763
- 1764
- 1765
- 1766
- 1767
- 1768 Romain Pierre Testuz, Yuliy Schwartzburg, and Mark Pauly. 2013. Automatic generation
of constructable brick sculptures. *Eurographics 2013-Short Papers* (2013), 81–84.
- 1769 Richard A Waltz and Jorge Nocedal. 2004. KNITRO 2.0 User's Manual. *Ziena Optimiza-
1770 tion, Inc.[en ligne] disponible sur http://www.ziena.com (September, 2010)* 7 (2004),
33–34.
- 1771 Xudong Yang, Yuan Zhou, Huichan Zhao, Weicheng Huang, Yifan Wang, K Jimmy Hsia,
and Mingchao Liu. 2023. Morphing matter: from mechanical principles to robotic
applications. (2023).
- 1772 Yinan Zhang and Devin Balkcom. 2016. Interlocking structure assembly with voxels.
In *2016 IEEE/RSJ International Conference on Intelligent Robots and Systems (IROS)*.
IEEE, 2173–2180.
- 1773 Tianyu Zhu, Zeng-Hao Xu, Ligang Liu, and Xiao-Ming Fu. 2023. Modeling with discrete
equivalence classes of planar quads. *Computers & Graphics* 115 (2023), 404–411.
- 1774 Henrik Zimmer, Marcel Campen, David Bommes, and Leif Kobbelt. 2012. Rationalization
of triangle-based point-folding structures. In *Computer Graphics Forum*, Vol. 31.
Wiley Online Library, 611–620.
- 1775 Henrik Zimmer, Florent Lafarge, Pierre Alliez, and Leif Kobbelt. 2014. Zometool shape
approximation. *Graphical Models* 76, 5 (2014), 390–401.
- 1776
- 1777
- 1778
- 1779
- 1780
- 1781
- 1782
- 1783
- 1784
- 1785
- 1786
- 1787
- 1788
- 1789
- 1790
- 1791
- 1792
- 1793
- 1794
- 1795
- 1796
- 1797
- 1798
- 1799
- 1800
- 1801
- 1802
- 1803
- 1804
- 1805
- 1806
- 1807
- 1808
- 1809
- 1810
- 1811
- 1812
- 1813
- 1814
- 1815
- 1816
- 1817
- 1818
- 1819
- 1820
- 1821
- 1822
- 1823
- 1824